Capture of antiprotons by some radioactive atoms and ions

James S. Cohen*
Theoretical Division, Los Alamos National Laboratory, Los Alamos, New Mexico 87545, USA
(Received 8 August 2003; published 3 February 2004)

Cross sections for antiproton capture are calculated using the fermion molecular dynamics method for ions of current interest in experiments determining nuclear structure of the radioactive nuclei ^{8}He, ^{11}Li, ^{11}Be, and ^{21}Mg. The cross sections for the corresponding neutral atoms are also calculated. It is found that, except for helium, the cross sections for the ion and neutral atom at usual capture energies are similar, i.e., neither the enhanced trajectory curvature nor the absence of the most weakly bound electron have great effect. The behavior of the cross sections is also analyzed at very low collision energies, where the ion cross sections go as $1/E$ and the neutral cross sections as $1/\sqrt{E}$.

DOI: 10.1103/PhysRevA.69.022501 PACS number(s): 36.10.−k, 25.43.+t, 21.10.Gv

I. INTRODUCTION

With the recently developed source of slow antiprotons (antiproton decelerator, AD at CERN) it is possible to do much more precise experiments with antiprotonic ($\bar{p}$) atoms [1,2] as well as with antihydrogen [3,4]. Previous experiments with antiprotonic atoms have observed the x-ray cascade [5] and spectroscopy of antiprotonic helium ($\alpha\bar{p}e$) [6] after capture, but were unable to measure the capture cross section itself or even the ratio of these cross sections for components in a target mixture. While experiments with other exotic atoms (negative muons μ^- and pions π^-) have measured the capture ratios for many mixtures [7], the capture cross sections have largely been left to theory. Some stopping times for low-energy ($v \lesssim 1$ a.u.) negative muons have been experimentally measured [8,9], but this time depends mainly on the slowing-down cross sections and not greatly on the capture cross section *per se*.

Recent theoretical calculations have indicated some dramatic effects of electron correlation and molecular structure that make the capture cross sections themselves of great current interest. However, the finite lifetime of the μ^- and π^- make direct measurements of the cross sections for capture very difficult. This limitation does not apply to $\bar{p}$. Modern theory predicts that capture occurs at collision energies on the order of the target electronic binding energies.

Previous calculations of exotic particle capture have been made only for neutral targets, though the main reason for this restriction was relevance to experiments. The incipient availability of trapped antiprotons changes this picture. In fact, in planned experiments with radioactive ions (RI) [10], the experimental roles of the $\bar{p}$ and ion may be reversed, with a beam of ions brought into a target of trapped antiprotons. Theoretically, of course, only the energy in the center-of-mass system matters. Ions provide some distinct experimental advantages: they are much more easily steered and contained than are neutral atoms.

The resulting antiprotonic atoms provide excellent probes of nuclear structure. First, the cascade x rays and Auger electrons exhibit nuclear size effects. Then the ultimate annihilation, which produces different pions [11] and residual nuclei depending on whether it occurs with a neutron or proton, provides information on the surface distribution of nucleons. Though the primary motivation for these experiments is characterization of radioactive nuclei, they will also provide a new opportunity for studying $\bar{p}$ capture. Beforehand, there is the need to have an estimate of the capture cross sections and collision energies at which captures occur in order to design the experiments. This information is needed to gauge both the characteristics required for the RI beam (E and $\Delta E/E$) and the magnitude of the anticipated signal, since exotic atom formation has not previously been observed with ionic targets. The cross section is also important for determining the acceptable background and minimum useful radioactive lifetime for a different experimental arrangement where the ion and the $\bar{p}$ may be placed in a nested trap.

We are presented with an interesting question: Is the ion cross section smaller or larger than the neutral cross section? In the absence of data, one can argue in both directions. On one hand, the positive ion will deflect the negative $\bar{p}$ to a closer approach and stronger interaction. On the other hand, there is one less electron to ionize and carry off the binding energy, and the remaining electrons are more tightly bound than in the corresponding neutral atom.

The leading candidates for the radiative ions are ^{8}He^{+}, ^{11}Li^{+}, ^{11}Be^{+}, ^{21}Mg^{+}, ^{78}Ni^{+}, and ^{100}Sn^{+} [12]. Previous calculations on the group of noble-gas atoms, He, Ne, Ar, Kr, and Xe, suggests that electron correlation is quite important and all the atomic electrons are involved to some extent in the capture process [13]. This might not be considered too surprising since the negative $\bar{p}$ is subject to an increasingly attractive potential all the way to the nucleus. However, it does present a theoretical challenge in that it means that a core potential for high-Z atoms would need to be chosen with great care, and no existing completely quantum-mechanical method is capable of treating the problem. The present work circumvents this problem by treating all electrons explicitly. For this reason, it is practical to treat only the lighter ions, ^{8}He^{+}, ^{11}Li^{+}, ^{11}Be^{+}, and ^{21}Mg^{+}, which should, in any event, be sufficient to exhibit the general characteristics. Similar calculations are done on the neutral atoms

*Electronic address: cohen@lanl.gov

TABLE I. FMD parameters. The associated first and second ionization potentials and total energies are compared with accurate values (experimental for the ionization potentials and Hartree-Fock for the total energy). In all cases, $\alpha_H=2.0$ and $\alpha_P=1.0$.

	FMD parameters		Associated energies (a.u.)					
	ξ_H	ξ_P	$I_1^{(\mathrm{FMD})}$	$I_1^{(\mathrm{expt})}$	$I_2^{(\mathrm{FMD})}$	$I_2^{(\mathrm{expt})}$	$E_{\mathrm{tot}}^{(\mathrm{FMD})}$	$E_{\mathrm{tot}}^{(\mathrm{H\text{-}F})}$
He	0.927	2.609	0.989	0.904	1.862	2.000	−2.85	−2.90
Li	0.925	4.005	0.198	0.198	2.860	2.780	−7.26	−7.48
Be	0.911	4.183	0.404	0.343	0.573	0.669	−14.5	−14.7
Mg	0.957	2.171	0.296	0.281	0.549	0.553	−193	−200
Mg′	0.919	2.238	0.281	0.281	0.456	0.553	−200	−200

to directly discern the difference in $\bar{p}$ capture by the atom and its ion.

II. THEORETICAL METHOD

A. Effective Hamiltonian

The antiproton capture is treated by solving Hamilton's classical equations of motion using an effective potential taking some essential quantum-mechanical effects into account. The effective potential is that proposed by Kirschbaum and Wilets (KW) for atomic structure [14]. In this model, pseudopotentials V_H and V_P constrain the quasiclassical dynamics to satisfy the Heisenberg uncertainty and Pauli exclusion principles, respectively. The resulting multielectron atom, which does not exist classically, is stabilized and possesses a shell structure [15]. Similar terms are included for the exotic atom structure, but have little effect since it is formed in highly excited states, which behave nearly classically according to the correspondence principle.

For an atomic target, the KW effective Hamiltonian is

$$H_{\mathrm{KW}}=H_0+V_H+V_P, \tag{1}$$

where

$$H_0=\frac{1}{2m_n}p_n^2+\frac{1}{2m_e}\sum_{i=1}^{N_e}p_i^2-\sum_{i=1}^{N_e}\frac{Ze^2}{r_{ni}}+\sum_{i=1}^{N_e}\sum_{j=i+1}^{N_e}\frac{e^2}{r_{ij}} \tag{2}$$

is the usual Hamiltonian and the added pseudopotentials are

$$V_H=\sum_{i=1}^{N_e}f(r_{ni},p_{ni};\xi_H,\alpha_H) \tag{3}$$

and

$$V_P=\sum_{i=1}^{N_e}\sum_{j=i+1}^{N_e}f(r_{ij},p_{ij};\xi_P,\alpha_P)\delta_{s_i,s_j}. \tag{4}$$

The sums are over the N_e electrons, r_{ni} (p_{ni}) is the relative distance (momentum) of electron i with respect to the nucleus n, r_{ij} (p_{ij}) is the relative distance (momentum) of electron j with respect to electron i, and s_i is the spin of electron i.

The form of the constraining potentials is taken as [14]

$$f(r_{\lambda\nu},p_{\lambda\nu};\xi,\alpha)=\frac{(\xi\hbar)^2}{4\alpha r_{\lambda\nu}^2\mu_{\lambda\nu}}\exp\left\{\alpha\left[1-\left(\frac{r_{\lambda\nu}p_{\lambda\nu}}{\xi\hbar}\right)^4\right]\right\} \tag{5}$$

in terms of the dimensionless parameters ξ and α, where the subscripts λ and ν designate pairs of particles with reduced mass $\mu_{\lambda\nu}$. The parameter ξ represents the size of the core (Heisenberg or Pauli), while α represents its hardness.

B. Parameters of the pseudopotentials

The values of α_H and α_P were fixed at 2.0 and 1.0, respectively, as recommended by Beck and Wilets [16]. Choice of the parameters ξ_H and ξ_P generally allow the matching of two physical characteristics of the actual atom *or* approximate matching of some set of characteristics. For negative-exotic-particle capture the single most important property is expected to be the target ionization energy. Higher ionization potentials and shell structure may also significantly affect the dynamics.

To ensure consistent treatment we employ the same pair of parameters for an element and all its ion stages. For balance, we chose to fit, in a least-squares sense, three characteristics, namely the first and second ionization potentials (I_1 and I_2) and the total electronic energy (E_{tot}) of each atom. Accuracy of the total energy implies correctness of the average ionization potential as well. For each pair of trial parameters in the nonlinear least-squares procedure, the coordinates and spins of all electrons are varied to minimize the energy given by the functional Eq. (1) (with $m_n\to\infty$), separately for the neutral ion, its singly charged ion, and its doubly charged ion. That is, the determination was actually carried out as a nested nonlinear least-squares procedure.

The resulting optimum parameters for He, Li, Be, and Mg are given in Table I. In all these cases, the minimum energy states were found to be the minimum spin states ($S=0$ for even numbers of electrons, $S=1/2$ for odd numbers of electrons), as is the case for the true quantum-mechanical ground states of these atoms and ions. This is not the result of any *a priori* constraint and, in fact, is not always the case with the KW ansatz [17]. The distances of the electrons from the nucleus for the atoms and first ions are shown in Fig. 1 (of course, the electrons have angular coordinates as well, so equal values of r_e do not mean the electrons are on top of each other). In the cases of He, Li, and Be, the α and β

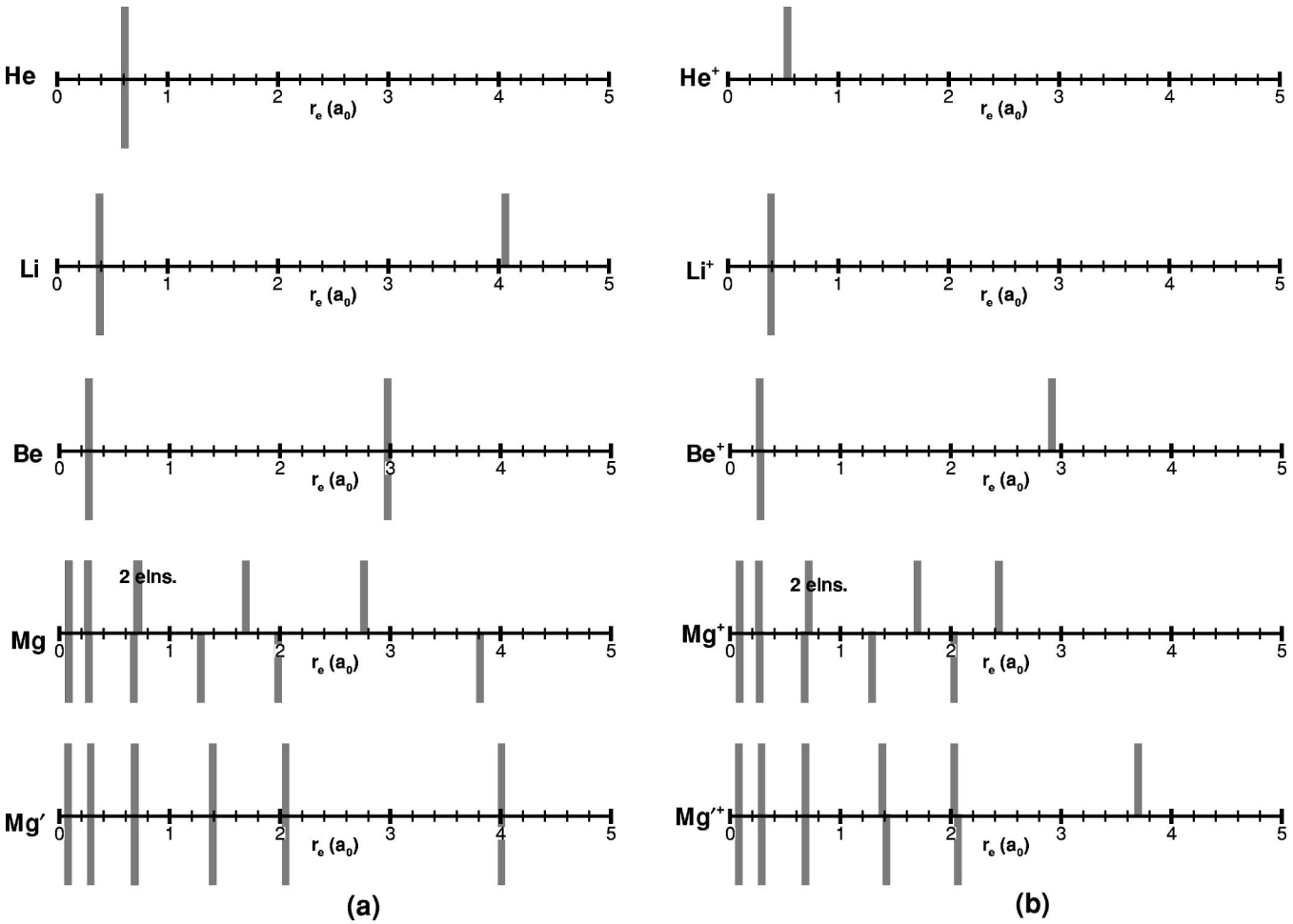

FIG. 1. Distances of the electrons from the nucleus in the initial KW configuration for (a) the atoms and (b) the singly charged ions. Both the broken-symmetry solution (Mg) and alternative symmetry solution (Mg′) are shown for magnesium (see text). The bars above the axis correspond to α (spin-up) electrons and the bars below the axis correspond to β (spin-down) electrons.

electrons are paired, i.e., they display the symmetry of the Hamiltonian, Eq. (1). However, the optimum solution for Mg displays broken symmetry for the more weakly bound electrons, unlike the ground-state quantum-mechanical configuration.

To better understand the source and effect of this broken symmetry solution, another optimization was done with a slightly different criterion, namely, matching of $E_{\rm tot}$ and I_1, without regard for I_2. This description allows $E_{\rm tot}$ and I_1 to be fit exactly. This solution is also given in Table I and Fig. 1, and we will refer to it as Mg′. It displays symmetry. While the associated I_2 is not as good as before, it is still reasonably close to the true value. This solution and the broken symmetry solution, both obtained without any constraints, are close in energy and the $\bar{p}$-capture dynamics is carried out with both to give some measure of the sensitivity of the cross section to the initial target configuration.

C. Monte Carlo calculation of the cross sections

Dynamics carried out with the KW ansatz for the atomic structure is known as fermion molecular dynamics (FMD) [18], with the Hamiltonian

$$H_{\rm FMD}=H_{\rm KW}+\frac{1}{2m_x}p_x^2+\sum_{i=1}^{N_e}\frac{e^2}{r_{ix}}-\frac{Ze^2}{r_{nx}}+f(r_{nx},p_{nx};\xi_H,\alpha_H), \tag{6}$$

where r_{nx} (p_{nx}) and r_{ix} (p_{ix}) are the relative distances (momenta) of the negative exotic particle x with respect to the nucleus n and electrons, respectively. The FMD method solves Hamilton's classical equations of motion,

$$\dot{\mathbf{r}}=\boldsymbol{\nabla}_p H_{\rm FMD}, \tag{7a}$$

$$\dot{\mathbf{p}}=-\boldsymbol{\nabla}_r H_{\rm FMD}, \tag{7b}$$

in terms of the laboratory-frame variables, $\mathbf{r}=\{\mathbf{r}_{\bar{p}},\mathbf{r}_{\rm nuc},\mathbf{r}_e^{(i)}\}$ and $\mathbf{p}=\{\mathbf{p}_{\bar{p}},\mathbf{p}_{\rm nuc},\mathbf{p}_e^{(i)}\}$, including all electrons, $i=1-N_e$.

The initial conditions of the target are set by performing a random Euler rotation of the target particles as a rigid body [19] with coordinates determined by the procedure in the preceding section. The $\bar{p}$ was normally started at a distance $10a_0$ away. At the lowest energy, calculations were also done with the initial distance increased to $20a_0$, but the cross sec-

TABLE II. Cross sections for capture of $\bar{p}$ by atoms.

$E_{\text{c.m.}}$ (a.u.)	σ_{capt} (units of a_0^2)				
	$\bar{p}+{}^{8}$He	$\bar{p}+{}^{11}$Li	$\bar{p}+{}^{11}$Be	$\bar{p}+{}^{21}$Mg	$\bar{p}+{}^{21}$Mg′
0.01	80.9±3.6	436±20	477±24	578±89	653±89
0.1	17.5±0.3	47±2	43.5±0.9	122±6	145±4
0.2	9.44±0.15	17.9±1.1	20.9±0.6	65.1±3.0	75.4±1.5
0.3	6.73±0.08	5.32±0.09	12.9±0.4		
0.4	5.37±0.06	3.23±0.07	8.53±0.24	35.7±2.3	39.2±2.1
0.5	4.47±0.07	2.42±0.07	5.15±0.13		
0.6	3.96±0.06	1.69±0.07	3.08±0.12	22.9±1.1	24.6±1.0
0.7	3.56±0.05	1.28±0.07	2.01±0.11		
0.8	3.24±0.05	1.04±0.07	1.38±0.11	16.1±0.8	17.1±0.7
0.9	2.95±0.05	0.81±0.06	1.26±0.11		
1.0	2.71±0.06	0.75±0.03	1.01±0.04	12.4±0.4	12.6±0.5
1.1	1.48±0.07	0.54±0.02	0.77±0.04		
1.2	0.85±0.02	0.49±0.02	0.64±0.04		
1.5	0.28±0.02	0.31±0.02	0.42±0.03	8.0±0.6	8.4±0.6
2.0	0.07±0.01	0.13±0.01	0.21±0.02	5.6±0.3	5.1±0.3
2.5	0.008±0.003	0.07±0.01	0.12±0.02		
3.0	0.002±0.002	0.03±0.01	0.08±0.01	2.89±0.13	2.60±0.13
4.0			0.010±0.004	1.85±0.16	1.67±0.16
6.0				0.73±0.05	0.67±0.04
8.0				0.37±0.04	0.42±0.04
10.0				0.24±0.04	0.28±0.04
12.0				0.13±0.03	0.19±0.03
15.0				0.06±0.02	0.10±0.02

tions were little changed. The trajectories were then run long enough to clearly identify whether or not the $\bar{p}$ was captured, but the final state was not otherwise characterized. Enough trajectories were run to get sufficient statistics at reasonable computational cost.

The trajectories were run in ranges of impact parameter b chosen by uniform sampling of $b^2 \in [(b_{i-1})^2,(b_i)^2]$. In the first range $[b_0,b_1]$, $b_0=0$ and b_1 was taken to be such that a small number (usually 2–3) of impact-parameter ranges will be required to converge the cross sections with $b_{i+1}=\sqrt{2}b_i$. The number of trajectories in each range was usually 500 for the He and Li targets, 200 for the Be target, and 100 for the Mg target.

In the ith range of impact parameter, the contribution to the cross section for a reaction R is given by

$$\sigma_R^{(i)}=\frac{N_i^{(R)}}{N_i^{\text{tot}}}\pi[(b_i)^2-(b_{i-1})^2] \tag{8}$$

with standard statistical error (assuming a binomial distribution) [20]

$$\Delta\sigma_R^{(i)}=\sigma_R^{(i)}\left(\frac{N_i^{\text{tot}}-N_i^{(R)}}{N_i^{\text{tot}}N_i^{(R)}}\right)^{1/2}, \tag{9}$$

where $N_i^{(R)}$ is the number of trajectories in which R occurred out of the total N_i^{tot} trajectories run with $b\in[b_{i-1},b_i]$. The integrated cross section is thus

$$\sigma_R=\sum_i \sigma_R^{(i)} \tag{10}$$

with estimated error

$$\Delta\sigma_R=\left(\sum_i (\Delta\sigma_R^{(i)})^2\right)^{1/2}. \tag{11}$$

III. RESULTS

The $\bar{p}$-capture cross sections, with statistical error bars, are given in Tables II and III for the neutral atoms and the ions, respectively. The cross sections for each neutral atom and ion are compared in Figs. 2(a)–(d) for He, Li, Be, and Mg. The most evident features are: (i) the magnitude of the cross section generally increases with increasing Z (except for He at $E_{\text{c.m.}}\approx 1$ a.u.), (ii) the highest energy at which capture occurs increases with increasing Z, and (iii) the difference between the neutral and ion cross sections diminishes with increasing Z. The increase in cross section and capture energy with Z is in keeping with the previous study of the noble-gas atoms. The decreasing effect of the most weakly bound atomic electron is consistent with more electrons participating in the capture process.

TABLE III. Cross sections for capture of $\bar{p}$ by atomic ions.

	σ_{capt} (units of a_0^2)					
$E_{c.m.}$ (a.u.)	$\bar{p}+{}^8He^+$	$\bar{p}+{}^8He'^+$	$\bar{p}+{}^{11}Li^+$	$\bar{p}+{}^{11}Be^+$	$\bar{p}+{}^{21}Mg^+$	$\bar{p}+{}^{21}Mg'^+$
0.01	295±7	215±7	230±12	662±35	1335±130	1414±125
0.1	14.7±0.6	13.5±0.6	16.4±0.6	51±3	134±5	137±5
0.2	5.34±0.17	4.83±0.17	6.6±0.3	17.4±1.0	66.6±2.8	71.5±2.2
0.3	2.86±0.10	2.58±0.09	3.97±0.09	8.58±0.26		
0.4	1.69±0.08	1.70±0.08	2.70±0.08	4.70±0.16	33.7±2.4	35.2±2.3
0.5	1.06±0.07	1.01±0.07	1.81±0.07	3.19±0.13		
0.6	0.76±0.06	0.74±0.06	1.45±0.07	2.14±0.13	21.5±1.2	20.4±1.3
0.7	0.67±0.06	0.59±0.06	1.03±0.07	1.62±0.11		
0.8	0.45±0.05	0.38±0.05	0.86±0.06	1.26±0.11	16.5±0.7	15.5±0.8
0.9	0.26±0.02	0.27±0.02	0.62±0.06	0.94±0.10		
1.0	0.19±0.02	0.20±0.02	0.59±0.02	0.83±0.04	12.1±0.3	12.3±0.3
1.1	0.10±0.01	0.15±0.01	0.46±0.02	0.71±0.04		
1.2	0.08±0.01	0.11±0.01	0.41±0.02	0.53±0.04		
1.5	0.03±0.01	0.03±0.01	0.25±0.02	0.33±0.03	7.5±0.6	7.2±0.6
2.0		0.005±0.002	0.12±0.01	0.13±0.02	5.0±0.3	4.9±0.3
2.5			0.06±0.01	0.09±0.02		
3.0			0.03±0.01	0.06±0.01	2.64±0.13	2.42±0.13
4.0			0.003±0.002	0.006±0.003	1.76±0.16	1.48±0.16
6.0					0.76±0.05	0.67±0.05
8.0					0.35±0.04	0.42±0.04
10.0					0.21±0.04	0.28±0.04
12.0					0.15±0.03	0.18±0.03
15.0					0.08±0.02	0.09±0.03

For He^+, which has only the one tightly bound electron, the cross section is much less than for He except at very low energy where the effect of trajectory curvature dominates. For the bigger atoms, the ion cross section is moderately smaller than the neutral cross section except at quite low energies. In any case, trajectory curvature due to the long-range Coulomb attraction between the negative antiproton and positive ion must dominate below some energy, but this energy can be seen to be quite low.

For helium, one might question the use of the average parameter ξ_H, given in Table I, for the one-electron He^+ ion, which, like the hydrogen atom, can be treated with the exact I_2 using the original KW parameter $\xi_H=(1+1/2\alpha_H)^{-1/2}$. Thus we have redone the $\bar{p}+He^+$ calculations with this parameter and show the results for comparison (designated "He'^+"). It can be seen that the two results are generally in quite good agreement. At the highest collision energies the treatment with the exact $I_2=2.0$ does yield a somewhat larger cross section than the treatment with $I_2=1.86$, as might be expected from the higher ionization potential taking more energy from the incident antiproton. However, the ion cross section depends smoothly on energy and is negligible at relative energies in excess of the ionization energy.

This behavior is in contrast to capture by the neutral atom. For the He atom the effect of quasiadiabatic ionization is evident (strictly adiabatic ionization is impossible since the $\bar{p}+$He united-atom limit, H^-, is bound). The average energy of the ejected electrons is $\sim$0.1 a.u., although occasionally electrons with energies as high as 0.6 a.u. are seen. The cross section is fairly flat at energies somewhat less than I_1, with what energy dependence there is being largely due to trajectory curvature. The cross section then decreases rapidly at $E>I_1$, indicating both that the ejected electron carries off relatively little kinetic energy *and* that ionization of the second electron is unlikely (the latter is already suggested by the smallness of the $\bar{p}+He^+$ capture cross section at these energies).

The cross section calculated for $\bar{p}$ capture by He^+ at the lowest energy (0.01 a.u.) should be viewed with some caution. A significant number of the the $\bar{p}$ are temporarily captured in two-particle (Feshbach-like) resonances. This may be problematic if no real quantum-mechanical states exist at such energies; i.e., this mechanism could be a classical artifact.

It might be considered somewhat surprising that the $\bar{p}+$Li and $\bar{p}+Li^+$ capture cross sections, shown in Fig. 2(b), are so similar, even though $I_2 \gg I_1$. The reason is that, except at the lowest energies, capture by the neutral entails ionization of two electrons. There is only slight evidence of adiabatic-ionization-like behavior in the capture cross section, which can be seen in a change in the sign of $d^2\sigma/dE^2$ at $E\approx I_1=0.20$ a.u., even though this is a case where strictly adiabatic ionization could, in principle, occur since the united-atom limit, He^-, is unbound. As in adiabatic ionization, the average kinetic energy of the ejected electron is

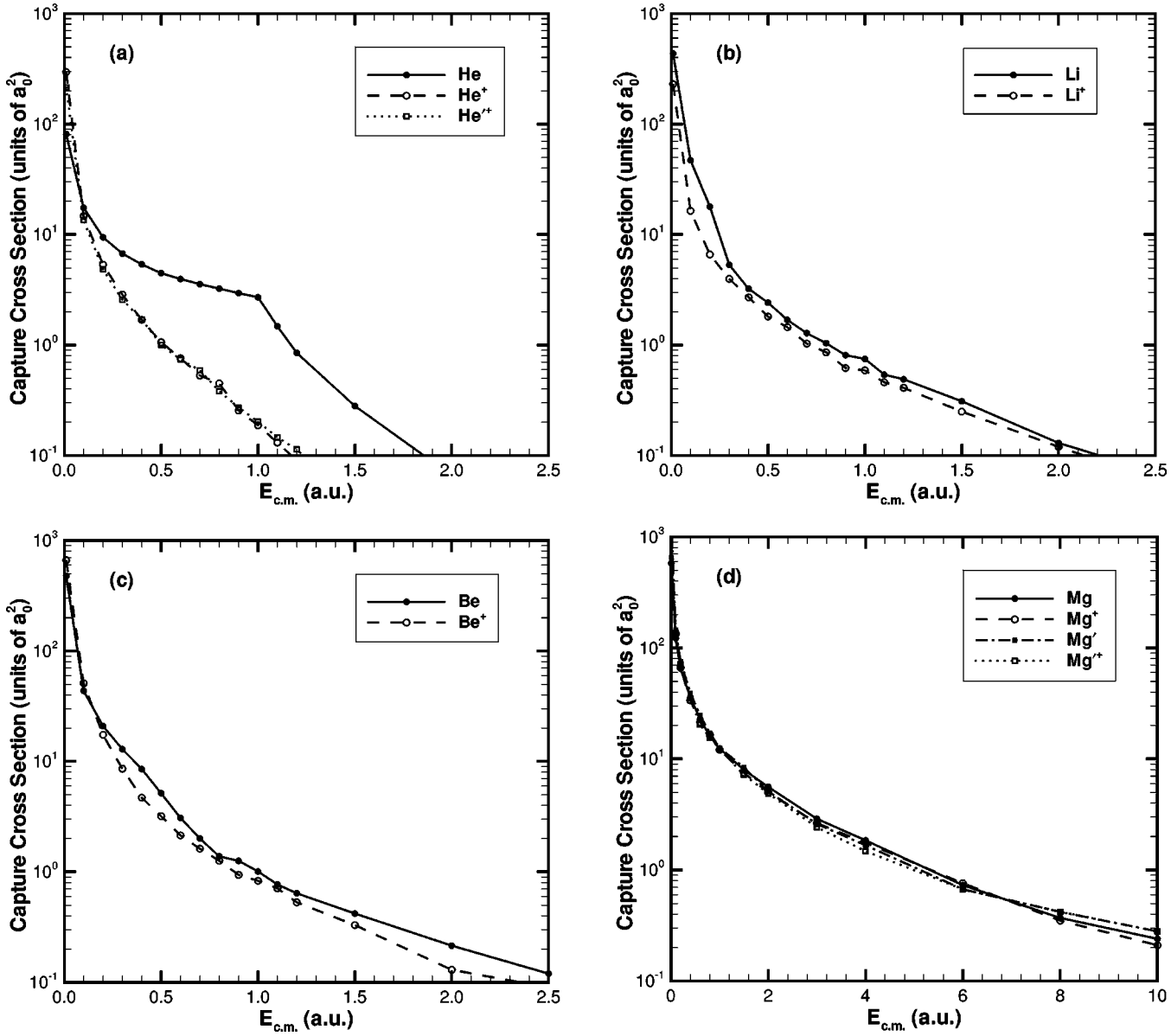

FIG. 2. Antiproton capture cross sections as a function of relative energy for the neutral and ion targets of (a) ^{8}He, (b) ^{11}Li, (c) ^{11}Be, and (d) ^{21}Mg. The solutions using the alternative KW configurations for He^+, Mg, and Mg^+ (designated by a prime) are shown for comparison.

relatively small ($\sim$0.1 a.u.). Even at the lowest collision energy calculated, 0.01 a.u., the ion cross section is still smaller than the neutral cross section. This shows that most of the deflection at this energy still occurs at distances smaller than that of the 2*s* orbital of Li, so screening by the outer electron is ineffective and deflection is similar for the atom and ion.

The relevant electronic structure of Be would seem to be quite different from Li. The most weakly bound two electrons of Be reside in the same shell, rather than in different shells, and have similar ionization energies, while these two ionization energies of Li are extremely different. Nonetheless, the $\bar{p}$ capture cross sections for Be and Be^+, shown in Fig. 2(c), are qualitatively similar to those for Li and Li^+. As with Li, there is only a hint of a kink in the $\bar{p}$+Be capture cross section at $\sim$0.4 a.u., which would be a sign of quasiadiabatic ionization. The average energy of the ejected electrons is $\sim$0.15 a.u., a bit higher than in the cases of He and Li.

The $\bar{p}$ capture cross sections of Mg and Mg^+ were carried out with the two different KW representations discussed in Sec. II B and yield the results shown in Fig. 2(d). Except at the lowest energies ($E_{\mathrm{c.m.}}<0.1$ a.u.), the atom and ion cross sections are almost the same. Enhancement by trajectory curvature approximately doubles the ion cross sections at $E_{\mathrm{c.m.}}=0.1$ a.u., and its influence can be expected to continue to grow at still lower energies.

Except possibly at the highest energies, $E_{\mathrm{c.m.}}>10$ a.u., the two representations give essentially the same result. This insensitivity is gratifying considering that the KW configuration of the outer electrons in the two configurations, desig-

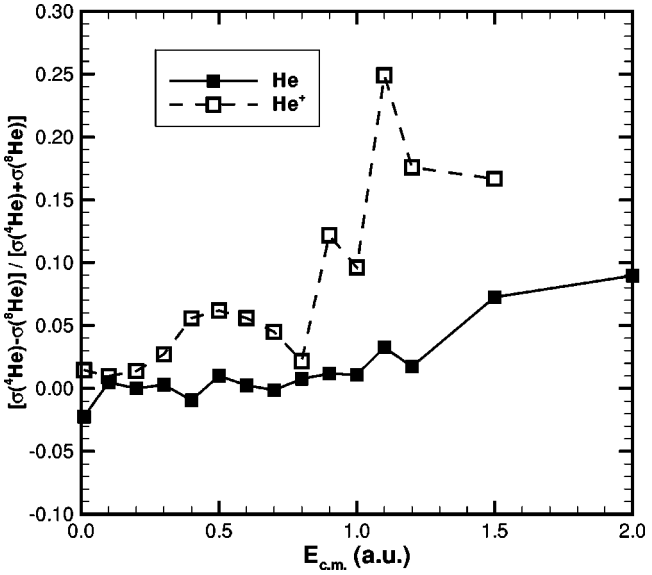

FIG. 3. Isotope effect on the antiproton capture cross sections for He and He^+.

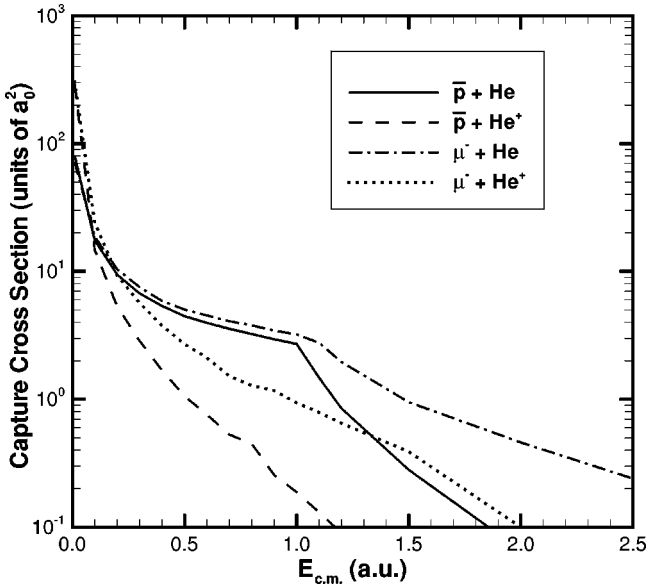

FIG. 4. Comparison of the cross sections for $\bar{p}$ and μ^- capture by ^{8}He and $^8He^+$.

nated "Mg" and "Mg′" in Fig. 1(a), appear to be so different. Even so, the energies of the two configurations are similar and apparently freely mix once the collision adds some energy to the electronic motion.

The cross sections for the magnesium target are considerably larger than those for the lighter elements and reach much higher collision energies. The energies of the ejected electrons are also about an order of magnitude higher than in the case of the lighter elements. However, it should be noted that these electron energies are affected by both the antiproton capture and subsequent Auger interactions, and there is no physical way to clearly separate these two mechanisms. Hence the observed electron energies will depend to some extent on how long the trajectories are integrated. Ultimately all electrons would be ionized though the quasiclassical treatment would not be adequate for the final steps in this cascade [21].

All the above calculations were done using the actual masses of the radioactive ions of current experimental interest. Generally the capture cross sections are not expected to depend strongly on the isotopic mass in the center-of-mass system. The lightest element considered, helium, can be expected to exhibit the greatest effect. The difference between ^{8}He and normal ^{4}He is shown in Fig. 3. The precision of the isotope effect determined in this way can be expected to be better than the separate error bars of the two isotopes might suggest, since the same initial conditions are used for both; however, it is not easy to quantify this correlation and the precision might best be gauged by the smoothness of the result as a function of collision energy. The calculated cross section for the lighter isotope is generally the larger, as expected. The isotope effect on capture of the neutral can be seen to be quite small, of the order of 1%. Due to the increased deflection by the long-range Coulomb potential, the isotope effect on capture by the ion is greater, possibly as much as $\sim$10% for He^+. For heavier elements, the isotope effect should be negligible for present purposes.

The mass effect of the projectile is greater. This effect has been studied in previous work on μ^- and $\bar{p}$ capture by the noble-gas elements as well as by the hydrogen molecule. There would seem to be little prospect for experiments on capturing the finite-lifetime μ^- by radioactive ions, but this theoretical comparison may shed some light on the dynamics of the capture process. The calculated cross sections for capture of μ^- and $\bar{p}$ by ^{8}He and ^{4}He are compared in Fig. 4. At the higher energies the muonic cross sections are considerably larger than the antiprotonic cross sections. This difference is due to the greater nonadiabatic effect with the lighter muon. For the neutral target, the difference is mainly at $E_{\mathrm{c.m.}} > I_1$ since the quasiadiabatic picture is a reasonably good description at $E_{\mathrm{c.m.}} < I_1$ in either case. For the ion target, the difference is large except at the smallest energies. At very low energies the cross sections for the muon and antiproton, as a function of center-of-mass system energy, are almost the same. In the adiabatic-ionization picture with trajectory curvature [22,23], they would be precisely the same.

IV. DISCUSSION AND CONCLUSION

The antiproton capture cross sections for ions with nuclear charge $Z>2$ have been found to be similar to the corresponding cross sections for the neutral atom. The effect of the increased trajectory curvature due to the long-range Coulomb attraction between the ion and antiproton is important only at very low collision energies ($E_{\mathrm{c.m.}} \lesssim 0.01$ a.u.), but, except for helium, the absence of the most loosely bound electron does not greatly diminish the capture cross section. This is good news for the feasibility of experiments with radioactive ions.

It is anticipated that energies as low as $E_{\mathrm{c.m.}} = 0.1$ eV (≈ 0.004 a.u.) may be reached in the experiments with radioactive ions [12]. At sufficiently low energies the capture cross section is expected to behave approximately as $1/E_{\mathrm{c.m.}}$

for $\bar{p}$ capture by ions and as $1/\sqrt{E_{\text{c.m.}}}$ for $\bar{p}$ capture by atoms (see the Appendix). This behavior appears to have been reached at the lowest calculated energies for the ions, and this simple extrapolation of the calculated FMD cross sections should be adequate.

However, the extrapolation of the atomic cross sections to lower energies must be done with more care (no such experiments are anticipated since it would be much more difficult to provide such a slow neutral beam). At fairly low energies the atomic cross sections also tend to behave approximately as $1/E_{\text{c.m.}}$ for $\bar{p}$ capture, like the cross sections for ions. But, at still lower energies, a centrifugal barrier weakens the dependence to $1/\sqrt{E_{\text{c.m.}}}$ (see the Appendix). At these very low energies, the atomic polarizability essentially determines the cross section, which then no longer exhibits the characteristic increase with increasing Z.

The validity of the quasiclassical description at very low energies is in question for the neutral atom targets. A serious problem is that the atomic polarizability is not well treated by the FMD method. The true ground states of the atoms presently considered (He, Li, Be, and Mg) are S states and thus spherically symmetric. While the ensemble of KW configurations is spherically symmetric, individual configurations are not. This becomes more of a defect as the energy decreases, since then there is time for the atom to be reoriented to its most polarizable (minimum energy) state by the incoming negative projectile.

This observation also suggests a procedure for obtaining the cross section at such low energies. Because FMD overestimates the effective polarizability at very low energies, it also overestimates the capture cross section there. But the Langevin (classical orbiting) formula overestimates the cross section if taken to inappropriately high energies. Thus the magnitudes of the two calculations cross at some collision energy, and a sensible approach is to use the FMD result above the crossing energy and the Langevin result, Eq. (A8), below the crossing energy. The recommended switchover energies for the atoms considered, which have polarizabilities $\alpha(\text{He})=1.383$ [24], $\alpha(\text{Li})=161.8$ [25], $\alpha(\text{Be})=36.6$ [26], and $\alpha(\text{Mg})=75$ [27] (in a.u.), are ~ 0.12 a.u. for $\bar{p}+\text{He}$, ~ 0.006 a.u. for $\bar{p}+\text{Li}$, ~ 0.03 a.u. for $\bar{p}+\text{Be}$, and ~ 0.10 a.u. for $\bar{p}+\text{Mg}$. Thus at sufficiently low (though not ultimately low—see the Appendix) collision energies, the cross sections for neutral atoms are simply given in terms of the atomic polarizability with no dynamical calculation required. In principle, this value is an upper bound (neglecting tunneling) since it assumes ionization always occurs upon close approach, but existing calculations tend to validate this assumption.

ACKNOWLEDGMENTS

I thank Dr. Michiharu Wada and Dr. Yasunori Yamazaki for suggesting this problem and helpful discussions. This work was done under the auspices of the U.S. Department of Energy.

APPENDIX: EXTRAPOLATION OF CROSS SECTIONS TO VERY LOW ENERGIES

We offer plausible arguments for interpreting the capture cross sections at very low collision energies. The adiabatic-ionization model was introduced by Wightman [28], based on the observation by Fermi and Teller [29] that there exists a critical dipole strength for binding an electron. For collision of $\bar{p}$ with a hydrogen atom, this corresponds to a critical distance $R_c=0.639a_0$, inside which the $\bar{p}$-p can no longer adiabatically bind the electron. With allowance for trajectory curvature, but assuming that there is no insurmountable centrifugal barrier outside R_c, the adiabatic ionization cross section at energy $E_{\text{c.m.}}$ is given by [22,23]

$$\sigma_{\text{AI}}=\frac{\pi R_c^2}{E_{\text{c.m.}}}\left(E_{\text{c.m.}}+\frac{1}{R_c}-0.5\right). \tag{A1}$$

Though the adiabatic-ionization model strictly applies only to neutral targets and then only when an electron in the united-atom limit of the $\bar{p}$ and the atom is unbound (e.g., H and Li), other cross sections tend to exhibit its form at low energies. We will make a heuristic generalization of this model. Suppose there exists a diabatic potential curve of the incident system ($\bar{p}+A$ or $\bar{p}+A^+$) that crosses the potential curve for the final state ($\bar{p}+A^+$ or $\bar{p}+A^{2+}$, respectively) at some $R=R_c$. Further suppose that the potential energy can be taken to be approximately $-Z_{\text{eff}}/R$. Then the quasiadiabatic ionization cross section is given by

$$\sigma_{\text{QAI}}=\pi b_c^2, \tag{A2}$$

where b_c satisfies

$$-\frac{Z_{\text{eff}}}{R_c}+\frac{b_c^2 E_{\text{c.m.}}}{R_c^2}=E_{\text{c.m.}}-I, \tag{A3}$$

and I is the ionization potential of the target. This yields

$$\sigma_{\text{QAI}}=\frac{\pi R_c^2}{E_{\text{c.m.}}}\left(E_{\text{c.m.}}+\frac{Z_{\text{eff}}}{R_c}-I\right). \tag{A4}$$

If we make the further assumption, which can be verified by the result, that $Z_{\text{eff}}/R_c \gg I$, then

$$\sigma_{\text{QAI}}\sim\frac{\pi R_c Z_{\text{eff}}}{E_{\text{c.m.}}} \text{ as } E_{\text{c.m.}}\to 0. \tag{A5}$$

We regard R_c here as a parameter. Mainly we want to use this form to extrapolate to lower energy, so the significant point is the $1/E_{\text{c.m.}}$ dependence. In the case of collision with a *positive ion*, the asymptotic potential is $-1/R$, so there are no long-range potential barriers and

$$\sigma_{\text{capt}}^{(\text{ion})}\approx\sigma_{\text{QAI}} \text{ as } E_{\text{c.m.}}\to 0. \tag{A6}$$

However, for a neutral target, the asymptotic potential is $-\alpha/(2R^4)$, where α is the polarizability of the target atom, and a centrifugal barrier may exist outside R_c that will limit

the cross section for collisions at sufficiently low energy. The classical orbiting model applies to this situation (tunneling is expected to have little effect). Using the effective potential for impact parameter b,

$$V_{\rm eff} = -\frac{\alpha}{2R^4} + \frac{b^2 E_{\rm c.m.}}{R^2}, \tag{A7}$$

and setting $dV_{\rm eff}/dR = 0$ and $V_{\rm eff} = E_{\rm c.m.}$ yields the Langevin cross section

$$\sigma_{\rm orb} = \pi b_{\rm orb}^2 = \pi \left(\frac{2\alpha}{E_{\rm c.m.}} \right)^{1/2}. \tag{A8}$$

The classical orbiting model requires that many angular-momentum partial waves occur, i.e.,

$$L_{\rm orb} = b_{\rm orb} p_{\rm rel} = \left(\frac{2\alpha}{E_{\rm c.m.}} \right)^{1/4} (2\mu E_{\rm c.m.})^{1/2} \gg 1, \tag{A9}$$

where μ is the reduced mass [30]. This condition is satisfied as long as $E_{\rm c.m.} \gg (8\alpha\mu^2)^{-1}$, which is typically $\sim 10^{-8}$ a.u. and much lower than any collision energy presently contemplated. Thus, at very low, though not ultimately low [31], energies the relevant cross section is

$$\sigma_{\rm capt}^{\rm (atom)} \approx \min(\sigma_{\rm QAI}, \sigma_{\rm orb}) \quad \text{as} \quad E_{\rm c.m.} \to \sim 0. \tag{A10}$$

This model is apropos to the low-energy limit for capture by *neutral* atomic targets; i.e., extrapolation to very low energies should be made by the dependence $1/\sqrt{E_{\rm c.m.}}$. However, it should be noted that it assumes the potential $-\alpha/(2R^4)$ and this asymptotic form of the potential breaks down at finite distances, especially for negative projectiles (see, e.g., the accurate result for the $\bar{p}+$H potential [23]).

[1] J. Eades and F.J. Hartmann, Rev. Mod. Phys. **71**, 373 (1999).
[2] Y. Yamazaki, Hyperfine Interact. **138**, 141 (2001).
[3] M. Amoretti *et al.*, Nature (London) **419**, 459 (2002).
[4] G. Gabrielse *et al.*, Phys. Rev. Lett. **89**, 233401 (2002).
[5] C.J. Batty, in *Antiproton-Nucleon and Antiproton-Nucleus Interactions*, edited by F. Bradamante, J.-M. Richard, and R. Klapisch (Plenum, New York, 1990), p. 251.
[6] T. Yamazaki *et al.*, Nature (London) **361**, 238 (1993).
[7] D. Horváth and R.M. Lambrecht, *Exotic Atoms* (Elsevier, Amsterdam, 1984).
[8] H. Anderhub *et al.*, Phys. Lett. **101B**, 151 (1981).
[9] P. Wojciechowski *et al.*, Hyperfine Interact. **82**, 127 (1993).
[10] M. Wada and Y. Yamazaki, Nucl. Instrum. Methods (to be published).
[11] W.M. Bugg, G.T. Condo, E.L. Hart, H.O. Cohn, and R.D. McCulloch, Phys. Rev. Lett. **31**, 475 (1973).
[12] M. Wada (private communication).
[13] J.S. Cohen, Phys. Rev. A **65**, 052714 (2002).
[14] C.L. Kirschbaum and L. Wilets, Phys. Rev. A **21**, 834 (1980).
[15] J.S. Cohen, Phys. Rev. A **51**, 266 (1995).
[16] W.A. Beck and L. Wilets, Phys. Rev. A **55**, 2821 (1997).
[17] J.S. Cohen, Phys. Rev. A **57**, 4964 (1998).
[18] L. Wilets and J.S. Cohen, Contemp. Phys. **39**, 163 (1998), and references therein.
[19] J.S. Cohen, Phys. Rev. A **56**, 3583 (1997).
[20] R. Abrines and I.C. Percival, Proc. Phys. Soc. London **88**, 861 (1966).
[21] K.J. LaGattuta (unpublished).
[22] J.S. Cohen, Phys. Rev. A **27**, 167 (1983).
[23] J.S. Cohen, in *Electromagnetic Cascade and Chemistry of Exotic Atoms*, edited by L.M. Simons, D. Horváth, and G. Torelli (Plenum, New York, 1990), p. 1.
[24] A.D. Buckingham and P.G. Hibbard, Symp. Faraday Soc. **2**, 41 (1968).
[25] G.M. Stacey, Proc. Phys. Soc. London **88**, 897 (1966).
[26] J.S. Sims and J.R. Rumble, Phys. Rev. A **8**, 2231 (1973).
[27] W.C. Stwalley, J. Chem. Phys. **54**, 4517 (1971).
[28] A.S. Wightman, Phys. Rev. **77**, 521 (1950).
[29] E. Fermi and E. Teller, Phys. Rev. **72**, 399 (1947).
[30] This is the only place where the mass occurs, other than through the relative energy, so the formulas of this Appendix apply to the negative muon as well as to the antiproton. Except for $\bar{p}+$H, the reduced mass μ is essentially just the mass of the negative particle.
[31] A. Yu. Voronin and J. Carbonell, Phys. Rev. A **57**, 4335 (1998).